Received 3 December 2018
Revised 26 April 2019
Accepted 16 May 2019

Comparison of different vector Preisach models for the simulation of ferromagnetic materials

Michael Nierla and Michael Loeffler
Department of Electrical, Electronic and Communication Engineering, Friedrich-Alexander-University Erlangen-Nuremberg, Erlangen, Germany

Manfred Kaltenbacher
Institute of Mechanics and Mechatronics, Vienna University of Technology, Vienna, Austria, and

Stefan Johann Rupitsch
Department of Electrical, Electronic and Communication Engineering, Friedrich-Alexander-University Erlangen-Nuremberg, Erlangen, Germany

Abstract

Purpose – The numerical computation of magnetization processes in moving and rotating assemblies requires the usage of vector hysteresis models. A commonly used model is the so-called Mayergoyz vector Preisach model, which applies the scalar Preisach model into multiple angles of the halfspace. The usage of several scalar models, which are optionally weighted differently, enables the description of isotropic as well as anisotropic materials. The flexibility is achieved, however, at the cost of multiple scalar model evaluations. For solely isotropic materials, two vector Preisach models, based on an extra rotational operator, might offer a lightweight alternative in terms of evaluation cost. The study aims at comparing the three mentioned models with respect to computational efficiency and practical applicability.

Design/methodology/approach – The three mentioned vector Preisach models are compared with respect to their computational costs and their representation of magnetic polarization curves measured by a vector vibrating sample magnetometer.

Findings – The results prove the applicability of all three models to practical scenarios and show the higher efficiency of the vector models based on rotational operators in terms of computational time.

Originality/value – Although the two vector Preisach models, based on an extra rotational operator, have been proposed in 2012 and 2015, their practical application and inversion has not been tested yet. This paper not only shows the usability of these particular vector Preisach models but also proves the efficiency of a special stageless evaluation approach that was proposed in a former contribution.

Keywords Magnetic hysteresis, Everett function, Vector Preisach model, Material modelling, Computational electromagnetics, Vector vibrating sample magnetometer, Vector hysteresis

Paper type Research paper

COMPEL - The international journal for computation and mathematics in electrical and electronic engineering
Vol. 38 No. 5, 2019
pp. 1696-1710

0332-1649
DOI 10.1108/COMPEL-12-2018-0494

1. Introduction

The classical scalar Preisach model (SP) describes hysteretic material behavior along a preset direction of polarization. Thus, it can successfully be applied in ferroelectric sensor and actuator design where such a fixed direction is usually available (Kaltenbacher, 2015; Rupitsch, 2019; Wolf, 2014). However, in magnetic field computations, especially in those

involving moving parts, the precondition of a fixed polarization axis is seldom satisfied. For such applications, vector hysteresis models are demanded, which allow for a self-adjustment of the polarization direction. One of these models is the vector Preisach model developed by Mayergoyz (MVP) (Mayergoyz, 2003). It enables the simulation of isotropic and anisotropic materials by applying the scalar Preisach models into N angular directions in space. Unfortunately, this flexibility comes at the computational cost of multiple scalar models. Furthermore, the Preisach weights for the particular scalar models require additional derivation, even for isotropic materials (Bottauscio *et al.*, 1998).

Sutor *et al.* (2012) and Sutor *et al.* (2015) proposed two vector Preisach models (VPR), which are based on a supplementary rotational operator that is added to SP. This light-weight extension of SP is suitable for isotropic materials and has the advantage that the Preisach weights of SP can be reused without further computations. However, an efficient stageless evaluation of these models, i.e. an evaluation similar to the Everett function for SP, requires a more complex implementation as reported in (Nierla *et al.*, 2017).

In this work, we compare MVP and the two variants of VPR in terms of accuracy and computational costs. In Section 2, we will provide the basic formulation of the tested hysteresis models. Section 3 investigates on the influence of the N directions onto the accuracy of the Mayergoyz model and compares it to the other tested models. The computation costs for evaluation and inversion of MVP and VPR will be compared to the corresponding runtimes of SP in Section 4. The contribution closes in Section 5 with a summary of the most important findings, as well as an outlook for further work.

2. Mathematical formulation of tested models

This section covers a short mathematical overview of the tested models and their respective parameters. A profound description can be found in (Kaltenbacher, 2015; Mayergoyz, 2003; Rupitsch, 2019; Sutor *et al.*, 2012; Sutor *et al.*, 2015) and shall not be repeated in detail here.

2.1 Scalar Preisach (SP) model and analytic weighting function μ_{DAT}

The classical scalar Preisach (SP) model shall shortly be discussed below as it not only embodies the core of the Mayergoyz vector Preisach model (MVP) but also serves as a reference in terms of the subsequent comparison of computational costs.

SP follows a phenomenological approach to describe hysteretic material behavior along a prescribed direction $\overrightarrow{r}_{\mathrm{SP}}$. It is based on elementary rectangular hysterons $R_{\alpha,\beta}[x(t)]$, also called switching operators, that are given as:

$$R_{\alpha,\beta}[x(t)] = \begin{cases} +1 & x(t) > \alpha \\ -1 & x(t) < \beta \\ R_{\alpha,\beta}[x(t^-)] & \text{else} \end{cases} . \tag{1}$$

Thereby:

$$x(t) = \frac{X(t)}{X_{\mathrm{sat}}} = \frac{\overrightarrow{X}(t) \cdot \overrightarrow{r}}{X_{\mathrm{sat}}} \tag{2}$$

represents the normalized projection of the vector input quantity $\overrightarrow{X}(t)$ along the prescribed direction $\overrightarrow{r}_{\mathrm{SP}}$ at the current instance of time t. t^- marks the previous instance of time and α/β stand for the up-/down-switching thresholds, respectively. To model actual material

behavior, a weighting function $\wp_{SP}(\alpha, \beta)$ is introduced, such that the integral over all weighted switching operators

$$Y_{SP}[x(t)] = Y_{sat} \int_{\alpha=-1}^{1} \int_{\beta=-1}^{\alpha} \wp_{SP}(\alpha, \beta) R_{\alpha,\beta}[x(t)] \, d\beta \, d\alpha \tag{3}$$

best matches the measured data Y_{meas} in a least-squares sense. In this context, one usually makes the following two demands on $\wp_{SP}(\alpha, \beta)$:

(1) $0 \geq \wp_{SP}(\alpha, \beta) < 1$; and

(2) $\int_{\alpha=-1}^{1} \int_{\beta=-1}^{\alpha} \wp_{SP}(\alpha, \beta) \, d\beta \, d\alpha = 1$.

The first condition ensures a monotonic behavior of the model, whereas the second one will lead to the saturation value Y_{sat} when the projected input quantity reaches $X_{sat.}$ The first condition will oftentimes be violated when determining the weights from multiple first or second order reversal curve (FORC or SORC) measurements as used by (Hegewald *et al.*, 2008) and (Mayergoyz, 2003). An alternative to this FORC-based derivation is the usage of analytic functions such as Gaussian, Lorentzian and Super-Lorentzian functions (Azzerboni *et al.*, 2004), although these functions are not equally suitable for all kind of materials. For soft-magnetic materials, for example, a Gaussian function is less usable, whereas Lorentzian only work for this kind of material (Takacs, 2012). It is also possible to apply a hyperbolic distribution as a weighting function, in which case, SP transfers to the hyperbolic hysteresis model introduced by Takacs (Takacs, 2012). As the main focus of this manuscript lies in the comparison of MVP and the two variants of VPR as presented further below, any weighting function could have been applied for the later comparisons as long as it leads to an adequate representation of our measurement and is the same for all models. Thus, without loss of generality, we utilize the so-called μ_{DAT} function that is defined as (Sutor *et al.*, 2010):

$$\mu_{DAT}(\alpha, \beta) = \frac{A}{1 + \left\{ [(\alpha + \beta)\sigma]^2 + [(\alpha - \beta - h)\sigma]^2 \right\}^{\eta}} \tag{4}$$

with the four model parameters A, σ, h and η because it allows a suitable representation of our tested materials. Moreover, we consider the addition of an anhysteretic part:

$$y_{anhyst}[x(t)] = a \arctan(bx(t)) \tag{5}$$

as proposed by (Sutor *et al.*, 2010), to the output of the pure hysteresis operator, with a and b representing two extra material dependent parameter. Therefore, the overall utilized scalar model reads:

$$Y_{SP}[x(t)] = Y_{sat} \left[y_{anhyst}[x(t)] + \int_{\alpha=-1}^{1} \int_{\beta=-1}^{\alpha} \mu_{DAT}(\alpha, \beta) R_{\alpha,\beta}[x(t)] \, d\beta \, d\alpha \right]. \tag{6}$$

The total set $\{A, \sigma, h, \eta, a \text{ and } b\}$ of six model parameters is determined by least-squares fitting of SP to a measured major loop curve as shown in Section 3. Please note that the addition of the anhysteretic part (5) usually results in $\int_{\alpha=-1}^{1} \int_{\beta=-1}^{\alpha} \wp(\alpha, \beta) \, d\beta \, d\alpha < 1$.

Finally, a vector output $\vec{Y}_{SP}[x(t)]$ is obtained by multiplying the scalar output value $Y_{SP}[x(t)]$ by $\vec{r}$.

2.2 Mayergoyz vector Preisach model

The vector Preisach model reported by Mayergoyz uses multiple instances of SP and applies them to each possible direction $\vec{r}$ of the halfcircle (2D) or hemisphere (3D) (Mayergoyz, 2003; Saitz, 2001). Using polar coordinates $(\rho, \varphi)/(\rho, \varphi, \theta)$ and setting $\vec{r} = \vec{e}_{\varphi}$ / $\vec{r} = \vec{e}_{\varphi,\theta}$, the vector output $\vec{Y}\left[\vec{X}(t)\right]$ for MVP computes as:

$$\vec{Y}^{\mathrm{2d}}_{\mathrm{MVP}}\left[\vec{X}(t)\right] = \int_{\varphi=0}^{\pi} Y_{\mathrm{SP},\varphi}\left[\frac{\vec{X}(t)}{X_{\mathrm{sat}}} \cdot \vec{e}_{\varphi}\right] \vec{e}_{\varphi}\, \mathrm{d}\varphi \tag{7}$$

$$\vec{Y}^{\mathrm{3d}}_{\mathrm{MVP}}\left[\vec{X}(t)\right] = \int_{\varphi=0}^{2\pi}\int_{\theta=0}^{\pi/2} Y_{\mathrm{SP},\varphi,\theta}\left[\frac{\vec{X}(t)}{X_{\mathrm{sat}}} \cdot \vec{e}_{\varphi,\theta}\right] \vec{e}_{\varphi,\theta} \sin(\theta)\, \mathrm{d}\theta\, \mathrm{d}\varphi \tag{8}$$

for 2D and 3D, respectively. $Y_{\mathrm{SP},\varphi}[\cdot]$ and $Y_{\mathrm{SP},\varphi,\theta}[\cdot]$ stand for SP in $\vec{e}_{\varphi}$ and $\vec{e}_{\varphi,\theta}$ direction. In general, each direction may have a unique scalar model, i.e. may use a unique weighting function $\wp_{\varphi}(\alpha, \beta)$ / $\wp_{\varphi,\theta}(\alpha, \beta)$ and also different anhysteretic curves. Thus, anisotropic material behavior can be modeled. However, the derivation of $\wp_{\varphi}(\alpha, \beta)$ / $\wp_{\varphi,\theta}(\alpha, \beta)$ is a non-trivial task that is described in detail in (Mayergoyz, 2003). Even for the isotropic case, where the weighting functions are the same in each spatial direction, their value is not identical to that of a pure scalar model. At least in the isotropic case, there exist analytic ways to transfer the weighting function from the pure scalar model $\wp_{\mathrm{SP}}(\alpha, \beta)$ to the vector model. For our contribution, we stick to 2D isotropic modeling. The considered analytic transformation of the weighting function was presented by Bottauscio *et al.* (Bottauscio *et al.*, 1998) and reads:

$$\wp_{\mathrm{MVP}}(\alpha, \lambda\,\alpha) = \begin{cases} \displaystyle\int_0^{\alpha} \frac{3s^2 \wp_{\mathrm{SP}}(s, \lambda\, s) + s^3 \dfrac{\partial}{\partial s} \wp_{\mathrm{SP}}(s, \lambda\, s)}{\pi \alpha^2 \sqrt{\alpha^2 - s^2}} \mathrm{d}s & \alpha \neq 0 \\ \dfrac{3}{4} \wp_{\mathrm{SP}}(0,0) & \alpha = 0 \end{cases} . \tag{9}$$

This transformation is based on the postulation that MVP should lead to the same result as SP when applied to a pure 1D signal along direction $\vec{r}_{\mathrm{SP}}$:

$$\vec{Y}^{\mathrm{2d}}_{\mathrm{MVP}}\left[\vec{X}(t)\right] \stackrel{!}{=} \vec{Y}_{\mathrm{SP}}\left[\vec{X}(t)\right] \quad \text{if } \vec{X}(t) = c(t)\, \vec{r}_{\mathrm{SP}} \quad . \tag{10}$$

It has to be pointed out that the presented transformation is applicable only to the pure weighting function, i.e. without considering anhysteretic parts in the scalar model. If isotropic anhysteretic parts are considered, the weighting function can be transformed as described above and the isotropic vectorial anhysteretic part:

$$\vec{y}_{\mathrm{anhyst,iso}}\left[\vec{X}(t)\right] = a \arctan\left(b \frac{\left\|\vec{X}(t)\right\|}{X_{\mathrm{sat}}}\right) \frac{\vec{X}}{\left\|\vec{X}\right\|} \tag{11}$$

is added outside of the integrals, where a and b can directly be taken from the scalar model. In case of anisotropic anhysteretic parts, the anhysteretic parts have to be contained inside the single scalar models and, thus, have to be considered during the weight transformation.

To use MVP in practice, the integrals over the halfspace have to be discretized. For the 2D case, N_φ discrete angular directions $\vec{e}_{\varphi_i}$ are required, whereas in 3D, even $N_\varphi \times N_\theta$ angles have to be considered, which obviously leads to a much higher computation cost for storage and evaluation of the 3D model. In 2D, the actual used vector Preisach model, including isotropic anhysteretic parts, reads:

$$\begin{aligned}\vec{Y}^{\mathrm{2d}}_{\mathrm{MVP}}\left[\vec{X}(t)\right] &\approx \vec{Y}^{\mathrm{2d}}_{\mathrm{MVP},N}\left[\vec{X}(t)\right] \\ &= Y_{\mathrm{sat}}\,\vec{y}_{\mathrm{anhyst,iso}}\left[\vec{X}(t)\right] \\ &+ \sum_{i=1}^{N} Y_{\mathrm{SP},\varphi_i}\left[\frac{\vec{X}(t)}{X_{\mathrm{sat}}}\cdot\vec{e}_{\varphi_i}\right]\vec{e}_{\varphi_i}\,\Delta\varphi_i,\end{aligned} \tag{12}$$

with $N = N_\varphi$ being the number of angular directions, $\vec{e}_{\varphi_i}$ and $\Delta\,\varphi_i$ the corresponding angular increments. Without loss of generality, we have used N equally distributed angular directions i.e. $\Delta\,\varphi_i = \Delta\,\varphi = \pi/N$ for all i. This is in accordance with Bottauscio *et al.*, 1998; Mayergoyz, 1986; Saitz, 2001, and has the advantage that no angular direction is preferred because of a larger weighting term. Unfortunately, any discretization will break the rotational symmetry of the continuous model, i.e. the output of the discrete model depends on the choice of a starting axis from which all other directions are derived. In practical finite element (FE) simulations, this issue can be addressed by choosing a different randomized starting axis at each element so that in average, the effect of the starting axis cancels out (Saitz, 2001). In Section 3.1, a short parameter study regarding the influence of the N directions as well as the choice of the starting axis upon the accuracy of the model is shown. For the remainder of this work, the x-axis was used as the default starting axis $\vec{r}_0$ for MVP as well as the prescribed direction $\vec{r}_{\mathrm{SP}}$ for SP.

2.3 Vector Preisach models based on rotational operators

In 2012 and 2015, Sutor *et al.* presented two variants of a light-weight vector Preisach (VPR) model, which is based on the addition of a so-called rotational operator $\vec{\chi}_{\alpha,\beta}[\cdot]$ to SP (Sutor *et al.*, 2012; Sutor *et al.*, 2015). Both variants of this vector model compute the vector output $\vec{Y}_{\mathrm{VPR}}[\cdot]$ to vector input data $\vec{X}(t)$ by:

$$\vec{Y}_{\mathrm{VPR}}\left[\vec{X}(t)\right] = Y_{\mathrm{sat}}\int_{\alpha=-1}^{1}\int_{\beta=-1}^{\alpha}\wp(\alpha,\beta)\,\vec{\chi}_{\alpha,\beta}\left[x_{\mathrm{thres}}(t)\right]R_{\alpha,\beta}\left[x_{\|\alpha,\beta}(t)\right]\mathrm{d}\beta\,\mathrm{d}\alpha, \tag{13}$$

where $x_{\mathrm{thres}}(t)$ stands for the so-called rotational threshold and

$$x_{\|,\alpha,\beta}(t) = \frac{\vec{X}(t)}{\|\vec{X}(t)\|}\cdot\vec{\chi}_{\alpha,\beta}\left[x_{\mathrm{thres}}(t)\right] \tag{14}$$

for the normalized projection of $\vec{X}(t)$ onto $\vec{\chi}_{\alpha,\beta}[\cdot]$. The setting rules for $\vec{\chi}_{\alpha,\beta}[\cdot]$ and the computation of $x_{\mathrm{thres}}(t)$ differ between the two variants and, thus, will be reported in detail in the corresponding subsections. The basic idea of the vector extension of SP is as follows:

The rotational threshold $x_{\text{thres}}(t)$, which is related to the amplitude of $\vec{X}(t)$, causes a (partial) alignment of $\vec{Y}[\cdot]$ to the outer field $\vec{X}(t)$. This angular alignment gets expressed by the rotational operator $\vec{\chi}_{\alpha,\beta}[\cdot]$. The actual strength of the alignment is reflected by the value of the corresponding scalar switching operator $R_{\alpha,\beta}[.]$.

The two main advantages of this model are as follows:

- First, the model is directly applicable to both 2D and 3D cases, as only the directions, which are handled by $\vec{\chi}_{\alpha,\beta}[\cdot]$, have to be extended by one additional entry.
- Second, the weighting function $\wp(\alpha, \beta)$ as well as possible anhysteretic parameters coincide with the one of SP and therewith require no additional transformation as it is the case of MVP[1].

However, this model is (currently) limited to isotropic materials and cannot directly make use of the efficient Everett function for evaluation (Nierla *et al.*, 2017).

2.3.1 Setting rules for vector Preisach model – classic version. In the originally proposed variant of VPR, called classic version and abbreviated VPRc in the following, the rotational operator $\vec{\chi}_{\alpha,\beta}[\cdot]$ is defined as (Sutor *et al.*, 2012):

$$\vec{\chi}_{\alpha,\beta}\left[x_{\text{thres}}(t)\right] = \begin{cases} \vec{d}^{c} & x_{\text{thres}}(t) > \alpha \\ \vec{d}^{c} & -x_{\text{thres}}(t) < \beta \\ \vec{\chi}_{\alpha,\beta}\left[x_{\text{thres}}(t^{-})\right] & \text{else} \end{cases} \tag{15}$$

with

$$x_{\text{thres}}(t) = \|\vec{X}(t)\|^{k^{c}} \tag{16}$$

and

$$\vec{d}^{c} = \frac{\vec{X}(t)}{\|\vec{X}(t)\|} \tag{17}$$

In this variant, the rotational operator at α, β will perfectly align with the applied outer field $\vec{X}(t)$ if $\|\vec{X}(t)\|^{k^{c}}$ surpasses the corresponding values of α, β. The material-dependent rotational resistance k^{c} influences how fast the model aligns with the applied field.

2.3.2 Setting rules for vector Preisach model – revised version. The modified variant as presented in (Sutor *et al.*, 2015), subsequently called revised version and abbreviated by VPRr, computes $\vec{\chi}_{\alpha,\beta}[\cdot]$ by:

$$\vec{\chi}_{\alpha,\beta}\left[x_{\text{thres}}(t)\right] = \begin{cases} \vec{d}^{r} & x_{\text{thres}}(t) > \max(\|\alpha\|, \|\beta\|) \\ \vec{\chi}_{\alpha,\beta}\left[x_{\text{thres}}(t^{-})\right] & \text{else} \end{cases} \tag{18}$$

with

$$x_{\text{thres}}(t) = k^{r}\|\vec{X}(t)\| \tag{19}$$

and

$$\overrightarrow{d^r} = \begin{cases} \overrightarrow{\chi}_{\alpha,\beta}\left[x_{\text{thres}}(t^-)\right] & \psi < \Delta\phi \\ [\mathbf{R}(\psi - \Delta\phi)]\overrightarrow{\chi}_{\alpha,\beta}\left[x_{\text{thres}}(t^-)\right] & \text{else} \end{cases} . \tag{20}$$

Here,

$$\psi = \text{angle}\left(\overrightarrow{\chi}_{\alpha,\beta}\left[x_{\text{thres}}(t^-)\right], \overrightarrow{X}(t)\right) \tag{21}$$

is the angle difference between the last occupied state and the currently applied field. The expression

$$[\mathbf{R}(\psi - \Delta\phi)] \tag{22}$$

defines a rotation matrix that rotates $\overrightarrow{\chi}_{\alpha,\beta}\left[x_{\text{thres}}(t^-)\right]$ by $(\psi - \Delta\ \phi)$ degree towards $\overrightarrow{X}(t)$ with

$$\Delta\phi = \Delta\phi_0\left(1 - \frac{\|\overrightarrow{X}(t)\|}{X_{\text{sat}}}\right) \tag{23}$$

marking a remanent angular distance that vanishes towards saturation. Owing to the extended setting rules and the addition of another material dependent parameter $\Delta\phi_0$, called angular distance, VPRr allows a more advanced description of rotating effects compared to VPRc but also requires additional computational effort.

3. Comparison between measurements and simulations

Before comparing the different models with respect to their computational costs, we first have to determine appropriate parameter sets that lead to comparable results. All tested models (SP, MVP, VPRc, VPRr) utilized the same parameter set $\{A, h, \sigma, \eta, a, b\}$ for the analytic Preisach weight function μ_{DAT} which was obtained from a least-squares fitting of measured major loop curves. These measurements were performed on a sputtered cylindrical $Fe_{49}Co_{49}V_2$ specimen of 6.5 μm height and 8.5 mm diameter using a vector vibrating sample magnetometer (VVSM), which is a standard vibrating sample magnetometer (VSM) as described in (Fiorillo, 2010) that was extended by two transversal coils perpendicular to the excitation axis. Figure 1 shows the measured magnetic polarization $J_{\text{P,meas}}$ of the specimen as well as the simulated values $J_{\text{P,SP}}$ resulting from SP for the obtained parameter set. Table I lists the corresponding fitted material parameters $\{A, h, \sigma, \eta, a, b\}$ In case of MVP, the resulting Preisach weights were transformed using (9).

3.1 Mayergoyz vector Preisach model – influence of N on accuracy and runtime

The angular accuracy of MVP was tested by computing the polarization for different values of N as well as different starting axis $\overrightarrow{r}_0$ and comparing the results to a reference solution obtained for $N = 101$ and $\overrightarrow{r}_0 = x$-axis. Figure 2 (middle part) shows the maximal relative deviation from the reference solution for a down-spiraling input signal as displayed in the upper part of Figure 2 in dependence of N and $\overrightarrow{r}_0$. As one can observe, the angular resolution reaches acceptable accuracy already for a low number of N in the range 5-10. The starting axis $\overrightarrow{r}_0$ does not exhibit a visible influence on the maximal deviation.

The lower part of Figure 2 depicts the required central processing unit (CPU) times for the evaluation of MVP relative to the CPU times for SP. As expected, the evaluation times of MVP increase nearly linear with N and require around N times as long as SP. The minor influence of $\vec{r}_0$ on the evaluation time results from the natural variation in CPU performance.

In Figure 3, the approximation of a measured remanence drop is considered. Such a remanence drop is achieved by bringing a specimen from saturation to remanence, rotating it by 90° and then saturating it perpendicular to the remanent polarization. In theory, the remanent polarization should vanish if the applied perpendicular field reaches physical saturation. In the case of our tested $Fe_{49}Co_{49}V_2$ specimen, we were not able to reach full physical saturation because of the lack of applicable field strength. Instead, only the so-called technical saturation $H_{\mathrm{sat,techn}}$ could be obtained which was used in the Preisach models as value for H_{sat}.

Figure 3 displays the measured remanence drop and the simulated curves from MVP using different values of N. One can see that the measured specimen roughly drops to 0.0 at H_{sat}, but in the shown case, it is more because of measurement fluctuations than complete depolarization. Extrapolating the measured curve would lead to a small remanent

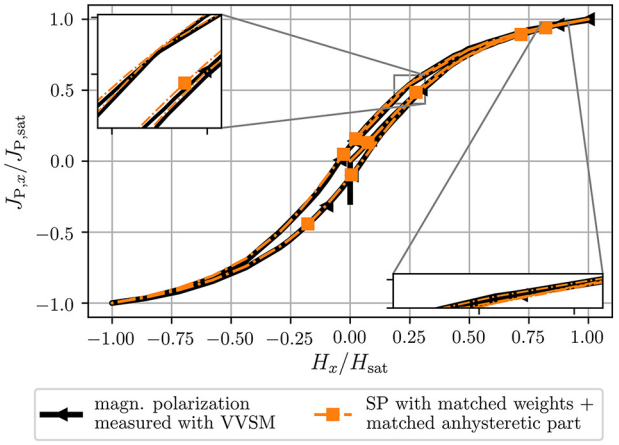

Figure 1. Measured and simulated major loop for a sputtered, cylindrical $Fe_{49}Co_{49}V_2$ specimen of 6.5 μm height and 8.5 mm diameter

Table I. Derived model parameters (A, h, σ, η) for analytic μ_{DAT} function as well as anhysteretic contribution (a, b) for a sputtered, cylindrical $Fe_{49}Co_{49}V_2$ specimen of 6.5 μm height and 8.5 mm diameter

A	h	σ	η	a	b
2.75182	0.08409	5.25757	1.59801	0.34709	4.74110

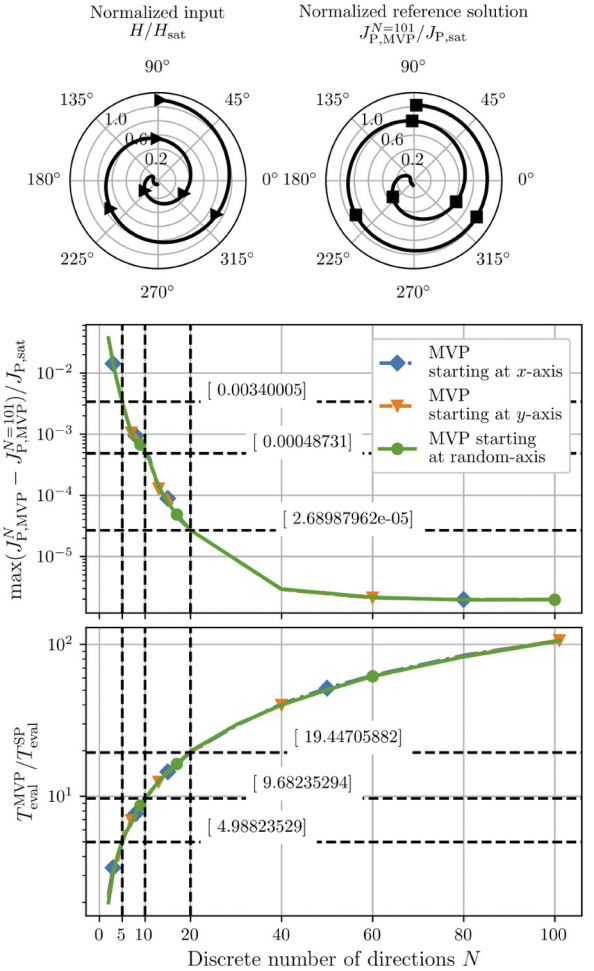

Notes: Upper part: applied down-spiraling input as well as reference solution $J^{N=101}_{P,MVP}$ computed by MVP with $N = 101$ and starting axis $\vec{r}_0 = x$-axis; Middle part: maximal difference in computed polarization J_P between MVP and the reference solution as a function of N and $\vec{r}_0$ for a down-spiraling input signal. Values are normalized to $J_{P,sat}$; Lower part: evaluation time for MVP T^{MVP}_{eval} relative to evaluation time for SP T^{SP}_{eval} as a function of N and $\vec{r}_0$

Figure 2.
Influence of N on accuracy and runtime of MVP

polarization perpendicular to the applied excitation. This effect is also visible for MVP but the actual retained value is much larger compared to the tested specimen and strongly depends on N. For values of $N \geq 20$, the simulated curves converge to the same remanent value at $H_{sat.}$ The remanent polarization of MVP comes from the scalar sub-models that

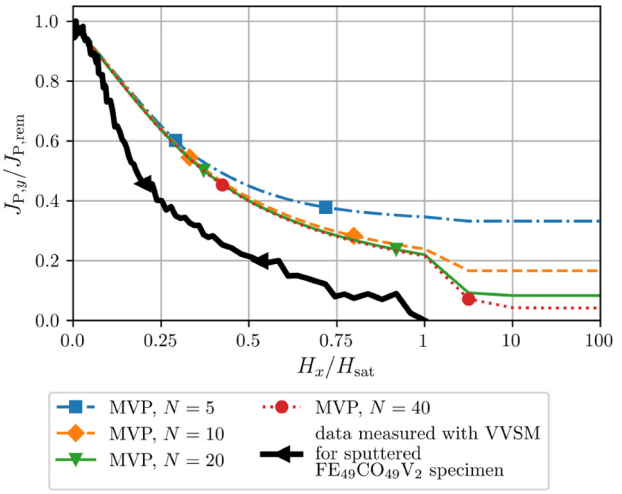

Notes: MVP retains a remanent polarization, which does not match the measured polarization of the tested $Fe_{49}Co_{49}V_2$ specimen

Figure 3. Measured and simulated depolarization process by applying a strong magnetic field perpendicular to the remanent magnetic polarization (remanence drop)

stand perpendicular on the excitation. These models receive an excitation of 0.0, independent on the strength of the applied field and thus, remain in remanence. For $N \to \infty$, the contribution of the perpendicular directions vanishes, such that for $H \to \infty$, the remanent polarization of MVP actually disappears. It has to be emphasized that the observed mismatch in retained remanent polarization highly depends on the tested specimen. For specimens with higher remanent polarization, MVP can lead to a very good matching.

3.2 Vector Preisach model – determination of additional vector parameters

The remanence drop from the previous section can be used to determine the additional material parameters k^c and k^r, $\Delta\phi_0$ for VPRc and VPRr, respectively (Sutor *et al.*, 2012). Figure 4 shows the measured and simulated curves of VPRc and VPRr for optimized parameters $k^c \approx 1.37$ and $k^r \approx 2.44$, $\Delta\phi_0 \approx 16.94^\circ$. Unlike MVP, neither VPRc nor VPRr retain remanent values at $H_{sat,}$ which is a fundamental and intended property of this kind of vector model. For the tested specimen, a very good matching could be achieved with VPRr as the polarization nearly drops to 0.0 at $H_{sat,techn.}$ VPRc achieves acceptable matching only for the first steep part of the remanence drop.

3.3 Mayergoyz vector Preisach model and Vector Preisach model application to additional measurements

To investigate on the applicability of MVP, VPRc and VPRr to more practical scenarios, J_P was measured for the tested $Fe_{49}Co_{49}V_2$ specimen using a FORC that was applied under a stepwise back-and-forth rotation of the specimen. The resulting applied magnetic field projected onto an x–y coordinate system is displayed in the upper part of Figure 5. The middle and lower part of this figure show the resulting measured and simulated polarization values in x- and y-direction, respectively. Along the x-axis, all tested models lead to the same

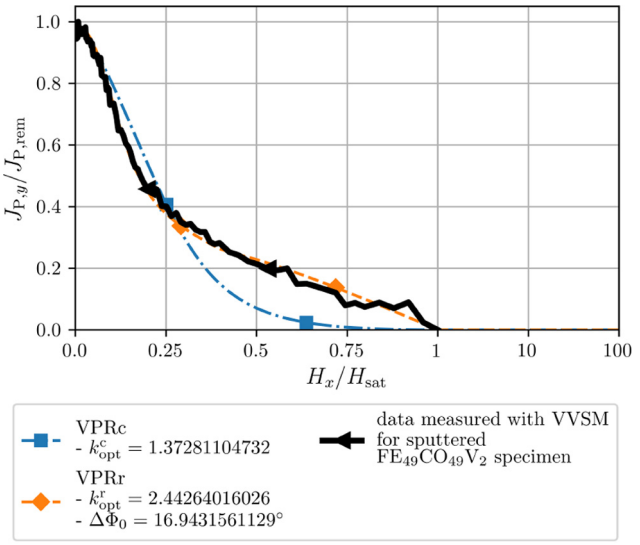

Figure 4.
Measured and simulated depolarization process by applying a strong magnetic field perpendicular to the remanent magnetic polarization (remanence drop)

Notes: VPRc and VPRr drop to 0 at technical saturation. VPRr allows for better matching because of additional parameter $\Delta\phi_0$

near-perfect match of the measured data. This is mostly because of the fact that the tested input signal is very similar to the major loop to which the Preisach weight function was matched. In that case, one can expect a very good agreement between measurements and simulations. Looking at the polarization along the *y*-axis, two aspects have to be highlighted. At first, the simulations lead to very similar polarization curves albeit the different matching of the remanence drop. Thereby, only VPRc shows a significant difference to the other vector models. Nevertheless, all vector models fail to predict the actual measured polarization curve for measurement steps 100-150 and 200-300. This is partially caused by the second aspect, which is the much stronger noise level along the *y*-axis. The noise and the drift along the *y*-axis stem from the transversal coils of the used VVSM, which measured $J_{P,y}$ to the largest part. These coils stand perpendicular to the applied field inside the VVSM and, thus, only measure remanent polarization. For the tested $Fe_{49}Co_{49}V_2$ specimen, the remanent polarization was quite weak, so that the induced voltages in the transversal coils were only slightly above noise level. Taking the named aspects into account, one can conclude that all three models are well applicable for practical purposes.

4. Runtime comparison between tested models

In the previous section, we showed that the three tested vector Preisach models suit for practical application. In this section, the actual computational cost in form of required evaluation and inversion time shall be compared. All retrieved runtimes are given as multiples of the runtime of SP to eliminate the effect of different hardware architectures. All models are implemented in our research FE code coupled field simulation (CFS++) (Kaltenbacher, 2010) (programming language C++). For the evaluation case, i.e. computing, $\vec{J}_P$ for a given $\vec{H}$, SP uses an efficient Everett function as described in (Kaltenbacher, 2015) and (Rupitsch, 2019). The implemented version of MVP internally stores N instances of SP

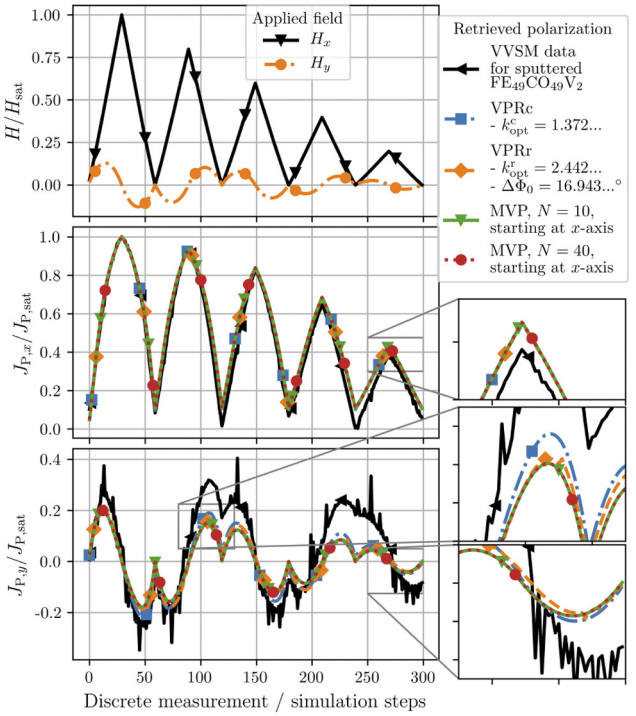

Notes: Upper part: applied magnetic field projected along x- and y-axis; Middle part: measured and simulated magnetic polarization along x-axis. All tested models lead to a nearly perfect match of the measured curve; Bottom part: measured and simulated magnetic polarization along y-axis. Deviation between measurements and simulations increases for diminishing excitation signals

Figure 5.
Comparison of different vector models for a rotated FORC signal

and executes them sequentially in a for-loop, thus utilizing the efficient Everett function during evaluation. Note that a parallel execution of this for-loop would have been possible, but was not performed here. The reason is the fact that in later FE simulations, each element (or even each integration point) has its own hysteresis model, which leads to an outer for-loop. Numerically, it is more efficient to parallelize this outer loop over the elements as it reduces the overhead for creating and synchronization of multiple threads. VPRc and VPRr exploit an efficient nested-list implementation as reported in (Nierla *et al.*, 2017), which is an extension of the Everett function for the vector case.

As common FE simulations for magnetics solve for $\overrightarrow{B} = \mu_0 \overrightarrow{H} + \overrightarrow{J}_P$, the Preisach models have to be inverted. This can be done by standard nonlinear solution techniques such as fixpoint iteration, Newton's method and Levenberg–Marquardt regularization (Dahmen and Reusken, 2008; Jin, 2010). For the following comparison, a standard Newton iteration scheme was used. In addition, an efficient Everett-based inversion for SP, which is described in detail in Rupitsch (2019), Wolf (2014) and Wolf *et al.* (2013), was tested. We want to point out that all

following evaluations and inversions were performed on a single element, i.e. no actual FE simulations were performed for the following comparisons. This treatment can be considered sufficient here, as the focus of this work lies in the comparison between measured and simulated material curves rather than the modeling of actual sensor or actuator behavior.

Figure 6 depicts from top to bottom the applied test signals for the runtime comparison as well as the required average CPU times for evaluation and model inversion. The obtained results enable the following observations.

Both evaluation and inversion times strongly depend on the applied input signal. This can easily be explained by the wipe-out principles of the Everett function on which all tested models are based. Shortly said, these wipe-out principles limit the input history that the Preisach model requires to represent hysteretic behavior to a list of dominant input minima and maxima. For oscillating input signals of decreasing amplitude, this list grows in size whereas it contains only very few entries for input signals with a low number of oscillations or for increasing amplitudes. The shorter this list, the faster the model can be evaluated. This explains well why the down-spiraling input signal leads to the highest computational effort.

Comparing the different vectors models, VPRc can both be evaluated and inverted fastest. Except for the down-spiraling test signal, it can even outperform the scalar model. VPRr performs similarly fast as VPRc for the decreasing sine signal but shows worse performance for the other tested signals, especially for the down-spiraling signal. This performance loss results from the increased costs for computing new states for the rotational operator as defined by equation (20). Nevertheless, VPRr proves to be at least competitive with MVP, even for $N = 3$, which showed to be insufficiently accurate. With increasing N, the computational costs for MVP increase nearly linearly, as already seen in section 3.1.

Finally, the rightmost columns show the superiority of an Everett-based inversion for SP. It outperforms the tested Newton-based inversion by a factor of eight or more, depending on the tested signal.

5. Conclusion and outlook

In this contribution, we compared the widely used Mayergoyz vector Preisach model (MVP) with two vector Preisach models VPRc and VPRr, which use a rotational operator to model vector hysteresis. The authors determined appropriate model parameters for a cylindrical $Fe_{49}Co_{49}V_2$ specimen by least-squares fitting of the model output to data obtained from a VVSM. All three models proved to be applicable to the measured data. However, the results obtained by MVP strongly depend on the number N of discrete angular directions, which are used to resolve the 2D halfspace. For nearly uni-axial excitation, a fairly small number $N \approx 10$ suffices but, especially in case of an excitation perpendicular to the current polarization state, $N > 20$ might be required. As each direction corresponds to a single scalar Preisach model, the computation cost roughly scales with N and, thus, becomes impracticable for large values of N. For 3D setups, this issue gets amplified by the necessity to resolve the additional spatial angle θ with N_θ directions, which in total will lead to $N \times N_\theta$ scalar models that make up MVP in 3D. The vector models VPRc and VPRr, on the other hand, can be expected to perform similarly for 2D and 3D setups since they just have to extend the used rotational operator by a single component. To test the actual applicability of the models, the authors compared MVP, VPRc and VPRr to additional VVSM measurements of a FORC-like agnetic field that was applied under a stepwise back-and-forth rotation of the specimen. Our investigations showed that VPRc and VPRr offer a computationally cheap alternative to MVP already for 2D setups while providing comparable (and partially even higher) accuracy. Future work will be dedicated to the analysis of the 3D case and FE simulations of actual sensors and actuators.

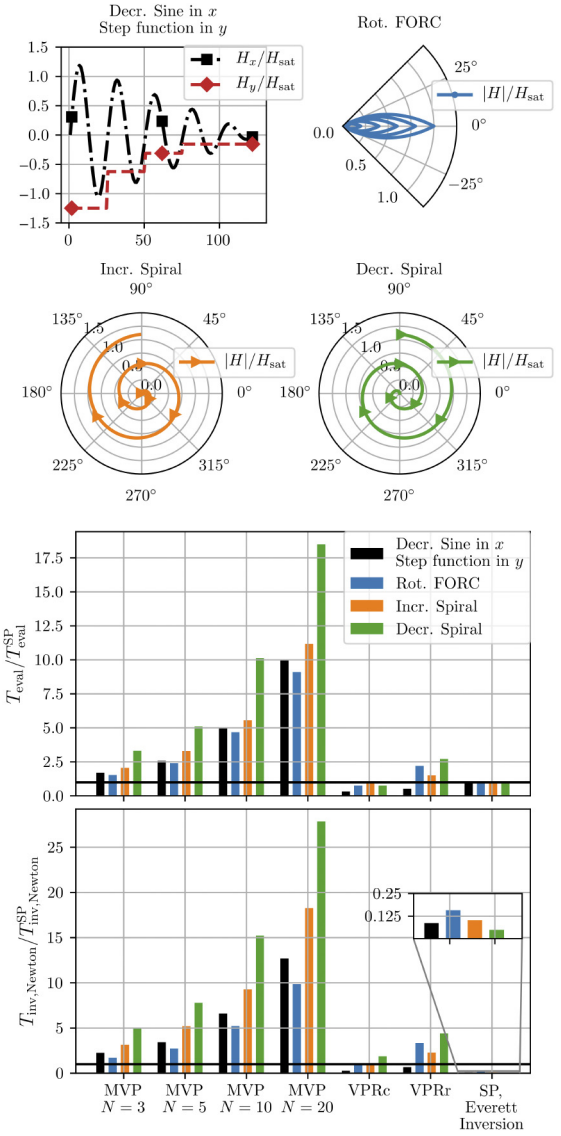

Notes: Upper part: applied input signals to tested Preisach models; Middle part: average CPU times for evaluating the tested Preisach models T_{eval} compared to the CPU times for SP T_{eval}^{SP} ; Lower part: average CPU times for inversion via Newton's method $T_{inv,Newton}$ compared to inversion times for SP via Newton's method $T_{inv,Newton}^{SP}$

Figure 6.
Runtime comparsion between scalar and vector Preisach models

Note

1. Anhysteretic parts are added like in the case of the MVP outside of the integrals.

References

Azzerboni, B., Carpentieri, M., Finocchio, G. and Ipsale, M. (2004), "Super-Lorentzian Preisach function and its applicability to model scalar hysteresis", *Physica B*, Vol. 343 No. 14.

Bottauscio, O., Chiarabaglio, D. and Ragusa, C. (1998), "Analysis of isotropic materials with vector hysteresis", *IEEE Transactions on Magnetics*, Vol. 34 No. 4.

Dahmen, W. and Reusken, A. (2008), *Numerik Für Ingenieure Und Naturwissenschaftler*, Springer, Berlin.

Fiorillo, F. (2010), "Measurements of magnetic materials", *Metrologia*, Vol. 47 No. 2.

Hegewald, T., Kaltenbacher, B., Kaltenbacher, M. and Lerch, R. (2008), "Efficient modeling of ferroelectric behavior for the analysis of piezoceramic actuators", *Journal of Intelligent Material Systems and Structures*, Vol. 19 No. 10.

Jin, Q. (2010), "On a regularized Levenberg-Marquardt method for solving nonlinear inverse problems", *Numerische Mathematik*, Vol. 115 No. 2.

Kaltenbacher, M. (2010), "Advanced simulation tool for the design of sensors and actuators", *Procedia Engineering*, Vol. 5

Kaltenbacher, M. (2015), *Numerical Simulation of Mechatronic Sensors and Actuators*, Springer, Berlin.

Mayergoyz, I.D. (1986), "Mathematical models of hysteresis", *IEEE Transactions on Magnetics*, Vol. 22 No. 5.

Mayergoyz, I.D. (2003), *Mathematical Models of Hysteresis and Their Applications*, Elsevier, New York, NY.

Nierla, M., Sutor, A., Rupitsch, S.J. and Kaltenbacher, M. (2017), "Stageless evaluation for a vector Preisach model based on rotational operators", *Compel – the International Journal for Computation and Mathematics in Electrical and Electronic Engineering*, Vol. 36 No. 5.

Rupitsch, S.J. (2019), *Piezoelectric Sensors and Actuators*, Springer, Berlin.

Saitz, J. (2001), "Magnetic field analysis of electric machines taking ferromagnetic hysteresis into account", *Acta Polytechnica Scandinavica*, Vol. 107.

Sutor, A., Bi, S. and Lerch, R. (2015), "Identification and verification of a Preisach-based vector model for ferromagnetic materials", *Journal of Applied Physics*, Vol. 118 No. 3.

Sutor, A., Kallwies, J. and Lerch, R. (2012), "An efficient vector Preisach hysteresis model based on a novel rotational operator", *Journal of Applied Physics*, Vol. 111 No. 7.

Sutor, A., Ruptisch, S.J. and Lerch, R. (2010), "A Preisach-based hysteresis model for magnetic and ferroelectric hysteresis", *Applied Physics A*, Vol. 100 No. 2.

Takacs, J. (2012), "The Everett integral and its analytical approximation", *Advanced Magnetic Materials*, Vol. 8, IntechOpen.

Wolf, F. (2014), "Generalisiertes Preisach-Modell für die Simulation und Kompensation der Hysterese piezokeramischer Aktoren", Phd thesis, FAU Erlangen-Nuremberg.

Wolf, F., Hirsch, H., Sutor, A., Rupitsch, S.J. and Lerch, R. (2013), Efficient Compensation of Nonlinear Transfer Characteristics for Piezoceramic Actuators, ISAF/PFM, Prague.

Corresponding author
Michael Nierla can be contacted at: michael.nierla@fau.de